Gulf Journal of Mathematics
Vol 21, Issue 2 (2025) 343-365

ISSN: 2309-4966
https://doi.org/10.56947/gjom.v21i2.3671

UAT TENSION B-SPLINE COLLOCATION METHOD FOR SOLVING A CLASS OF SINGULARLY PERTURBED CONVECTION-DIFFUSION PROBLEMS

MOHAMED CHAHER[1], ABDELLAH LAMNII[1]* and MOHAMED YASSIR NOUR[2]

Abstract. In this paper, we introduce a novel collocation method that utilizes Uniform Algebraic Trigonometric (UAT) tension B-splines to resolve a class of convection-diffusion problems with singular perturbations on a Shishkin mesh. We provide a rigorous analysis of the method's uniform convergence in relation to the perturbation parameter. To demonstrate the efficacy of the proposed approach, we conduct numerical experiments and compare the results with various benchmark problems from the literature. The findings highlight the accuracy and effectiveness of our method in addressing such problems.

Keywords. Convection-diffusion problem, UAT tension B-spline, Collocation method, Shishkin mesh
2020 Mathematics Subject Classification. Primary 46L55; Secondary 44B20

1. Introduction

Singularly perturbed boundary value problems (SPBVPs) frequently appear in various physical and engineering applications, such as civil engineering, computer science, heat transfer and aerodynamics, to name a few. These problems exhibit boundary layers due to small perturbation parameters, making them challenging to solve numerically. In certain regions of the domain, the solution exhibits rapid variations, while in others, it changes more gradually. Consequently, it is crucial to develop robust numerical methods that provide accurate error estimates independent of the small parameter. For a thorough explanation of how SPBVPs are treated analytically and numerically, readers are referred to the works of Robert et al. [16], Doolan et al. [4], Farrell et al. [5], Miller et al. [15], and Roos [17]. This study discusses the numerical solution of a class of convection-diffusion problems with singular perturbations:

$$L\,z\,(x) \equiv -\varepsilon\, z''\,(x) + p\,(x)\,z'\,(x) + q\,(x)\,z\,(x) = g\,(x)\,,\ \ x \in \Omega = [0,1]\,, \tag{1.1}$$

according to the boundary conditions

$$z\,(0) = A_0\ , z\,(1) = A_1, \tag{1.2}$$

Date: Received: Oct 8, 2025; Revised: Nov 6, 2025; Accepted: Nov 18, 2025.
* Corresponding author

where ε is a small positive perturbation parameter satisfying $0 < \varepsilon \ll 1$, A_0 and A_1 are constants, and L is a differential operator. Additionally, the functions $p(x)$, $q(x)$, and (x) are sufficiently smooth and satisfy the following conditions:

$$p(x) \geq p^* > 0 \quad \text{and} \quad q(x) \geq q^* > 0 \quad \text{for} \quad x \in [0, 1],$$

where p^* and q^* are positive constants. According to these conditions, the boundary layer will be situated close to $x = 1$, at the interval's right endpoint.

Numerous approaches have been proposed in the literature to address these types of problems. As an example, Kumar and Srinivasan [10] used second-order central difference schemes to create a novel adaptive mesh approach for convection-diffusion singularly perturbed problems. Kadalbajoo and Patidar [9] provided a succinct overview of numerical methods for resolving singularly perturbed problems. Lin et al. [14] developed a numerical method for resolving a singularly perturbed boundary value problem in biological science using B-splines. Alinia and Zarebnia [1] introduced a novel tension B-spline technique for boundary value problems with third-order self-adjoint singular perturbations, whereas, Kadalbajoo and Gupta [8] used a piecewise uniform Shishkin mesh to investigate a B-spline collocation approach for solving singularly perturbed convection-diffusion problems.

In this paper, we propose a new collocation method that employs Uniform Algebraic Trigonometric (UAT) tension B-splines to resolve a class of convection-diffusion problems with singular perturbations on a Shishkin mesh. The main contribution of this study lies in the use of boundary trigonometric tension B-splines on the right and left sides of the domain, which enhances the accuracy and performance of the proposed method. The structure of the paper is as follows. Section 2 presents analytical results for the continuous problem. In Section 3, we introduce the nonuniform Shishkin mesh and provide a straightforward representation of Uniform Algebraic Trigonometric tension B-splines of order 4 (UAT tension B-splines), which are used to resolve SPBVPs. In Section 4, the convergence analysis of the method is discussed, focusing on ε-uniform convergence in the maximum norm. In Section 5, we present three numerical examples to validate the method. The results and discussions of these examples are compared with those of the methods described in [14] and [8]. Finally, the conclusion is provided in Section 6.

2. Continuous problem

This section looks at the solution's and its derivatives' a priori bounds. The maximal norm for a given function $\zeta(x) \in C^k(\bar{\Omega})$ is defined as

$$\|\zeta\|_\infty = \max_{x \in \bar{\Omega}} |\zeta(x)|.$$

The differential operator L in (1.1) satisfies the following maximum principle on Ω.

Lemma 2.1 (Maximum Principle)**.** *Make the assumption that $\phi(0) \geq 0$ and $\phi(1) \geq 0$. For all $x \in \Omega$, $L\phi(x) \geq 0$ implies that $\phi(x) \geq 0$ for all $x \in \bar{\Omega}$.*

Proof. The proof is by contradiction.

Given $x^* \in \bar{\Omega} = [0,1]$ such that

$$\phi(x^*) = \min_{x \in \bar{\Omega}} \phi(x),$$

let's assume that $\phi(x^*) < 0$.

From the hypotheses, it follows that $x^* \notin \{0,1\}$. Therefore,

$$\phi'(x^*) = 0 \quad \text{and} \quad \phi''(x^*) \geq 0.$$

Now, consider the differential operator L evaluated at $x = x^*$:

$$\begin{aligned} L\phi(x^*) &= -\varepsilon\phi''(x^*) + p(x^*)\phi'(x^*) + q(x^*)\phi(x^*) \\ &= -\varepsilon\phi''(x^*) + p(x^*) \cdot 0 + q(x^*)\phi(x^*) \\ &= -\varepsilon\phi''(x^*) + q(x^*)\phi(x^*) < 0. \end{aligned}$$

This contradicts the assumption that $L\phi(x) \geq 0$ for all $x \in \Omega$.
Thus, $\phi(x^*) \geq 0$, and it follows that $\phi(x) \geq 0$ for all $x \in \bar{\Omega}$. □

Lemma 2.2. *Let z represent the SPBVPs 1.1 solution. Consequently, z satisfies:*

$$\|z(x)\| \leq \frac{\|g\|}{p^*} + \max\left(z(0), z(1)\right), \quad \forall x \in \bar{\Omega}.$$

Proof. Let's look at the barrier functions mentioned below:

$$\Phi^{\pm}(x) = x\frac{\|g\|}{p^*} + \max\left(z(0), z(1)\right) \pm z(x).$$

At $x = 0$, we obtain:

$$\Phi^{\pm}(0) = \max\left(z(0), z(1)\right) \pm z(0) = \max\left(|A_0|, |A_1|\right) \pm |A_0| \geq 0.$$

At $x = 1$, we obtain:

$$\Phi^{\pm}(1) = \frac{\|g\|}{p^*} + \max\left(z(0), z(1)\right) \pm z(1) = \frac{\|g\|}{p^*} + \max\left(|A_0|, |A_1|\right) \pm |A_1| \geq 0.$$

From (1.1), the differential operator L applied to $\Phi^{\pm}(x)$ yields:

$$\begin{aligned} L\Phi^{\pm}(x) &= -\varepsilon\left(\Phi^{\pm}(x)\right)'' + p(x)\left(\Phi^{\pm}(x)\right)' + q(x)\Phi^{\pm}(x) \\ &= p(x)\frac{\|g\|}{p^*} + q(x)\left[x\frac{\|g\|}{p^*} + \max\left(z(0), z(1)\right)\right] \pm Lz(x) \\ &= p(x)\frac{\|g\|}{p^*} + q(x)\left[x\frac{\|g\|}{p^*} + \max\left(z(0), z(1)\right)\right] \pm f(x) \\ &\geq \left[\|g\| \pm g(x)\right] + q(x)\max\left(z(0), z(1)\right) \\ &\geq 0. \end{aligned}$$

The proof is completed by the maximum principle, which asserts that $\Phi^{\pm}(x) \geq 0$ for all $x \in \bar{\Omega}$. □

Lemma 2.3. *Its derivatives and the solution $z(x)$, $x \in \bar{\Omega}$ of the SPBVPs 1.1 satisfy the following bounds:*

$$\left|z^{(\ell)}(x)\right| \leq C\left[1 + \varepsilon^{-\ell}\exp\left(\frac{-p^*(1-x)}{\varepsilon}\right)\right], \quad \ell = 0,1,2,3, \quad x \in \bar{\Omega}.$$

Proof. The proof follows in a similar manner to Lemma 8.1 in [15]. □

Theorem 2.4. *If the decomposition $z(x) = r(x)+s(x)$ is admitted by the solution $z(x)$ of problem 1.1, then for all ℓ, $0 \le \ell \le 3$, the regular component $r(x)$ satisfies*
.

$$\left|r^{(\ell)}(x)\right| \le C\left[1+\varepsilon^{-(\ell-2)}\exp\left(\frac{-p^*(1-x)}{\varepsilon}\right)\right], \quad \forall x \in \bar{\Omega} = [0,1],$$

and the singular component $s(x)$ satisfies

$$\left|s^{(\ell)}(x)\right| \le C\varepsilon^{-\ell}\exp\left(\frac{-p^*(1-x)}{\varepsilon}\right), \quad \forall x \in \bar{\Omega} = [0,1].$$

Proof. The detailed proof is provided in [8, 15]. □

3. Discrete problem

3.1. **The Shishkin mesh.** This section introduces the mesh selection approach used for solving problem (1.1). We focus on the piecewise uniform Shishkin mesh; for more details, see [8, 15].

In order to efficiently resolve the layer behavior, we utilize a Shishkin mesh designed to refine the grid near boundary layers. Let N be a positive integer divisible by 2. We partition the interval $\bar{\Omega} = [0,1]$ into two subdomains:

$$\Omega_\ell = [0, 1-\Upsilon] \quad \text{and} \quad \Omega_r = [1-\Upsilon, 1],$$

The choice of the transition point Υ based on ε and problem coefficients is as follows

$$\Upsilon = \min\left\{0.5, \Upsilon_0\, \varepsilon \ln N\right\},$$

where $\Upsilon_0 \ge \frac{2}{p^*}$ is a constant that doesn't depend on ε and N.

The mesh is constructed by placing uniform grids with $\frac{N}{2}$ intervals on each of the subintervals $[0, 1-\Upsilon]$ and $[1-\Upsilon, 1]$; see Figure 1. The step sizes are given by

$$h = \begin{cases} h_\ell = h_i = \frac{2(1-\Upsilon)}{N}, & \text{if } i = 1, 2, \ldots, \frac{N}{2}, \\ h_r = h_i = \frac{2\Upsilon}{N}, & \text{if } i = \frac{N}{2}+1, \frac{N}{2}+2, \ldots, N. \end{cases}$$

The distribution of the mesh points $\bar{\Omega}_N = \{x_i\}_{i=0}^N$ is as follows

$$x_i = \begin{cases} \frac{2(1-\Upsilon)}{N} i, & \text{if } i = 0, 1, \ldots, \frac{N}{2}, \\ (1-\Upsilon) + \frac{2\Upsilon}{N}\left(i - \frac{N}{2}\right), & \text{if } i = \frac{N}{2}+1, \frac{N}{2}+2, \ldots, N. \end{cases}$$

Thus, a uniform mesh is applied to each of these subintervals.
The following figure shows a Shishkin mesh for the one-dimensional problem 1.1 on the interval $[0,1]$, with $N = 16$.

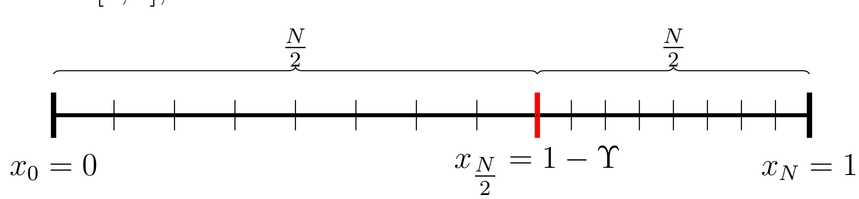

FIGURE 1. A Shishkin mesh for the one-dimensional problem (1.1) with $N = 16$.

3.2. Uniform Algebraic Trigonometric (UAT) Tension B-Spline Method.

In this part, the UAT tension B-splines of order 4 are briefly represented explicitly and their interesting properties are discussed. For more details, see [2, 6, 11, 12, 13, 18, 19].

We introduce the following notations to proceed:

Let $N = 2^k$ for a given positive integer $k > 2$. Consider the partition of $I = [0, 1]$:

$$\Delta = \begin{cases} x_{-3} = x_{-2} = x_{-1} = x_0 = 0, \\ x_i = ih, \quad i = 1, \ldots, N-4, \\ x_{N-3} = x_{N-2} = x_{N-1} = x_N = 1. \end{cases}$$

The trigonometric spline space of order 4 (UAT tension B-splines) is defined as follows:

$$\mathcal{S}_4 = \left\{ s \in \mathcal{C}^2(I) : s_{|_{[x_i, x_{i+1}]}} \in \Gamma_4 \right\},$$

where

$$\Gamma_4 = \text{span}\left\{1, x, \cos(\omega x), \sin(\omega x)\right\},$$

and ω is a positive real tension factor.

The space $\mathcal{S}_4$ has dimension $N + 3$, and the fourth-order trigonometric tension B-splines are defined by the following formula for $i = 0, 1, \ldots, N-4$:

$$TB_{i,4}(x) = \begin{cases} \frac{\omega(x-x_i) - sin\left[\omega(x-x_i)\right]}{2\,\omega\, h\,(1-cos(\omega h))}, & x \in [x_i, x_{i+1}[\,, \\ \frac{\omega(x_{i+2}-x) + 2\,\omega\,(x_{i+1}-x)\,cos(\omega h) - 2\,sin\left[\omega(x_{i+1}-x)\right] - sin\left[\omega(x_{i+2}-x)\right]}{2\,\omega\, h\,(1-cos(\omega h))}, & x \in [x_{i+1}, x_{i+2}[\,, \\ \frac{\omega(x-x_{i+2}) - 2\,\omega\,(x_{i+3}-x)\,cos(\omega h) + sin\left[\omega(x_{i+2}-x)\right] + 2\,sin\left[\omega(x_{i+3}-x)\right]}{2\,\omega\, h\,(1-cos(\omega h))}, & x \in [x_{i+2}, x_{i+3}[\,, \\ \frac{\omega(x_{i+4}-x) - sin\left[\omega(x_{i+4}-x)\right]}{2\,\omega\, h\,(1-cos(\omega h))}, & x \in [x_{i+3}, x_{i+4}[\,, \\ 0 & otherwise. \end{cases} \tag{3.1}$$

With the corresponding boundary trigonometric tension B-splines on the left and right, namely $TB_{-3,4}$, $TB_{-2,4}$, $TB_{-1,4}$, $TB_{N-3,4}$, $TB_{N-2,4}$, and $TB_{N-1,4}$, are defined as follows:

$$TB_{-3,4}\,(x) = \begin{cases} \frac{\omega(h-x) - sin[\omega(h-x)]}{\omega h - sin(\omega h)}, & x \in [x_0, x_1[\,, \\ 0 & otherwise. \end{cases}$$

$$TB_{N-1,4}\,(x) = \begin{cases} \frac{[\omega(x-h(n-1))] + sin[\omega(h(n-1)-x)]}{\omega h - sin(\omega h)}, & x \in [x_{N-1}, x_N[\,, \\ 0 & otherwise. \end{cases}$$

$$TB_{-2,4}\,(x) = \begin{cases} \frac{\omega x - sin(\omega h) + sin[\omega(h-x)]}{\omega h - sin(\omega h)} - \frac{2 sin[\omega(h-x)] + 2\,\omega\, x\, cos(h)}{2\,\omega h\, cos(\omega h) - 2\, sin(\omega h)} + & \\ \frac{2\, sin(\omega h) - \omega x + sin(\omega x)}{2\,\omega h\, cos(\omega h) - 2\, sin(\omega h)}, & x \in [x_0, x_1[\,, \\ \frac{[\omega(x-2h)] + sin[\omega(2h-x)]}{2\,\omega\, h\, cos(\omega h) - 2\, sin(\omega h)}, & x \in [x_1, x_2[\,, \\ 0 & otherwise. \end{cases}$$

$$
TB_{N-2,4}(x) = \begin{cases} \frac{[\omega(h(n-2)-x)]+sin[\omega(x-h(n-2))]}{2\,\omega h\,cos(\omega h)-2\,sin(\omega h)}, & x\in[x_{N-2},x_{N-1}[, \\ \frac{\omega(h(n-1)-x)\,sin(2\omega h)}{2(\omega h-sin(\omega h))(\omega\,h\,cos(\omega h)-sin(\omega h))}+ & \\ \frac{h\,(-2\,sin[\omega(x-h(n-1))]+sin[\omega(x-h(n-2))])}{2(\omega h-sin(\omega h))(\omega\,h\,cos(\omega h)-sin(\omega h))}+ & \\ \frac{\omega(x-nh)-sin(\omega h)(sin[\omega(nh-x)]+[\omega(h(n-2)-x)])}{2(\omega h-sin(\omega h))(\omega\,h\,cos(\omega h)-sin(\omega h))}, & x\in[x_{N-1},x_N[, \\ 0 & otherwise. \end{cases}
$$

$$
TB_{-1,4}\,(x) = \begin{cases} \frac{\omega x-sin(\omega x)}{2\,\omega\,h\,(cos(\omega h)-1)}+ & \\ \frac{2\,sin[\omega(h-x)]+2\omega x\,cos(\omega h)-2\,sin(\omega h)+\omega x-sin(\omega x)}{2\,\omega\,h\,cos(\omega h)-2sin(\omega h)}, & x\in[x_0,x_1[\,, \\ \frac{2\,\omega^2\,h(2h-x)cos^2(\omega h)-\omega(2h-x)(\omega h+sin(2\omega h))}{2\,\omega\,h\,(cos(\omega h)-1)(\omega\,h\,cos(\omega h)-sin(\omega h))}+ & \\ \frac{\omega\,h\,sin[\omega(2h-x)]+sin(\omega h)\,sin[\omega(h-x)]}{2\,\omega\,h\,(cos(\omega h)-1)(\omega\,h\,cos(\omega h)-sin(\omega h))}+ & \\ \frac{sin[\omega(2h-x)]+\omega h-\omega\,h\,cos(\omega h)\,sin[\omega(h-x)]+2\,sin[\omega(2h-x)]+\omega(x-h)}{2\,\omega\,h\,(cos(\omega h)-1)(\omega\,h\,cos(\omega h)-sin(\omega h))}, & x\in[x_1,x_2[\,, \\ \frac{\omega(x-3h)+sin[\omega(3h-x)]}{2\,\omega\,h\,(cos(\omega h)-1)}, & x\in[x_2,x_3[\,, \\ 0 & otherwise. \end{cases}
$$

$$
TB_{N-3,4}\,(x) = \begin{cases} \frac{\omega(h(n-3)-x)+sin[\omega(x-h(n-3))]}{2\,\omega\,h\,(cos(\omega h)-1)}, & x\in[x_{N-3},x_{N-2}[\,, \\ \frac{\omega(x-h(n-2))+sin[\omega(h(n-2)-x)]}{2\,\omega\,h\,cos(\omega\,h)-2sin(\omega h)}+\frac{sin(\omega h)-\omega h}{2\,\omega\,h\,(cos(\omega h)-1)}+ & \\ \frac{2\omega(h(n-2)-x)cos(\omega h)+sin(\omega h)+sin[\omega(x-h(n-1))]}{2\,\omega\,h\,(cos(\omega h)-1)}+ & \\ \frac{sin[\omega(x-h(n-2))]}{2\,\omega\,h\,(cos(\omega h)-1)}, & x\in[x_{N-2},x_{N-1}[\,, \\ \frac{\omega^2h(nh-x)cos(2\omega h)-\omega\,h\,sin[\omega(h(n-1)-x)]}{2\omega h(-1+cos(\omega h))(\omega\,h\,cos(\omega h)-sin(\omega h))}+ & \\ \frac{+sin[\omega(x-h(n-1))]-sin[\omega(x-h(n-2))]}{2\omega h(-1+cos(\omega h))(\omega\,h\,cos(\omega h)-sin(\omega h))}+ & \\ \frac{sin(2\omega h)+sin(\omega h)\,[\omega(x-h(n-2))]+sin[\omega(nh-x)]}{2\,\omega\,h\,(-1+cos(\omega h))(\omega\,h\,cos(\omega h)-sin(\omega h))}, & x\in[x_{N-1},x_N[\,, \\ 0 & otherwise. \end{cases}
$$

Trigonometric tension B-splines of order 4 retain all the desirable properties of classical polynomial B-splines, as discussed in [13, 18, 19]. In this paper, we highlight only a few of these properties.

- Local support: $TB_{i,k}\,(x) = 0$ for $x \notin [x_i, x_{i+k}]$.
- Positivity : $TB_{i,k}\,(x) \geq 0$, $\forall x \in [x_i, x_{i+k}]$.
- Linear independence: $TB_{-3,k}, \ldots, TB_{N-1,k}$ are linearly independent on $I = [0, 1]$.

Using the explicit formulas of the UAT tension B-splines of order 4, we provide in this section the expressions for the first and second derivatives of TB_i, for $i = -3, \ldots, N-1$. To simplify the calculations in the collocation method, we gather the values, first derivatives, and second derivatives of each TB_i at the nodes x_i.

$$
TB'_{i,4}\,(x) = \begin{cases} \frac{1-cos\,[\omega(x-x_i)]}{2\,h\,(1-cos(\omega h))}, & x\in[x_i,x_{i+1}[\,, \\ \frac{-1-2\,cos(\omega h)+2\,cos\,[\omega(x_{i+1}-x)]+cos\,[\omega(x_{i+2}-x)]}{2\,h\,(1-cos(\omega h))}, & x\in[x_{i+1},x_{i+2}[\,, \\ \frac{1+2\,cos(\omega h)-cos\,[\omega(x_{i+2}-x)]-2\,cos\,[\omega(x_{i+3}-x)]}{2\,h\,(1-cos(\omega h))}, & x\in[x_{i+2},x_{i+3}[\,, \\ \frac{-1+cos\,[\omega(x_{i+4}-x)]}{2\,h\,(1-cos(\omega h))}, & x\in[x_{i+3},x_{i+4}[\,, \\ 0 & otherwise. \end{cases} \tag{3.2}
$$

$$TB''_{i,4}(x) = \begin{cases} \frac{\omega \sin[\omega(x-x_i)]}{2h(1-\cos(\omega h))}, & x \in [x_i, x_{i+1}[\,, \\ \frac{2\omega \sin[\omega(x_{i+1}-x)]+\omega \sin[\omega(x_{i+2}-x)]}{2h(1-\cos(\omega h))}, & x \in [x_{i+1}, x_{i+2}[\,, \\ \frac{-\omega \sin[\omega(x_{i+2}-x)]-2\omega \sin[\omega(x_{i+3}-x)]}{2h(1-\cos(\omega h))}, & x \in [x_{i+2}, x_{i+3}[\,, \\ \frac{\omega \sin[\omega(x_{i+4}-x)]}{2h(1-\cos(\omega h))}, & x \in [x_{i+3}, x_{i+4}[\,, \\ 0 & otherwise. \end{cases} \tag{3.3}$$

The values of $TB_{i,4}$, $TB'_{i,4}$ and $TB''_{i,4}$ at the nodal points x_i, $i = -3, \ldots, N-1$, are provided in Tables 1 to 7.

TABLE 1. The values of $TB_{i,4}(x)$, $TB'_{i,4}(x)$ and $TB''_{i,4}(x)$ at the nodal points.

	x_i	x_{i+1}	x_{i+2}	x_{i+3}	x_{i+4}
$TB_{i,4}(x)$	0	η	κ	η	0
$TB'_{i,4}(x)$	0	-ρ	0	ρ	0
$TB''_{i,4}(x)$	0	σ	-2σ	σ	0

Where

$$\eta = \frac{\omega h - \sin(\omega h)}{4\omega h \sin^2\left(\frac{\omega h}{2}\right)}, \quad \kappa = \frac{-\omega h \cos(\omega h) + \sin(\omega h)}{2\omega h \sin^2\left(\frac{\omega h}{2}\right)},$$

$$\rho = \frac{1}{2h}, \quad \text{and} \quad \sigma = \frac{\omega \cot\left(\frac{\omega h}{2}\right)}{2h}.$$

TABLE 2. The values of $TB_{-3,4}(x)$, $TB'_{-3,4}(x)$ and $TB''_{-3,4}(x)$ at the nodal points.

	x_0	x_1	x_2	x_3	x_4
$TB_{-3,4}(x)$	1	0	–	–	–
$TB'_{-3,4}(x)$	ℓ_1	0	–	–	–
$TB''_{-3,4}(x)$	ℓ_3	0	–	–	–

TABLE 3. The values of $TB_{N-1,4}(x)$, $TB'_{N-1,4}(x)$ and $TB''_{N-1,4}(x)$ at the nodal points.

	x_{N-4}	x_{N-3}	x_{N-2}	x_{N-1}	x_N
$TB_{N-1,4}(x)$	–	–	–	0	1
$TB'_{N-1,4}(x)$	–	–	–	0	$-\ell_1$
$TB''_{N-1,4}(x)$	–	–	–	0	ℓ_3

Where

$$\ell_1 = \frac{-\omega + \omega \cos(\omega h)}{\omega h - \sin(\omega h)} \quad \text{and} \quad \ell_3 = \frac{\omega^2 \sin(\omega h)}{\omega h - \sin(\omega h)}.$$

TABLE 4. The values of $TB_{-2,4}(x)$, $TB'_{-2,4}(x)$ and $TB''_{-2,4}(x)$ at the nodal points.

	x_0	x_1	x_2	x_3	x_4
$TB_{-2,4}(x)$	0	e_1	0	$-$	$-$
$TB'_{-2,4}(x)$	$\ell_2 = -\ell_1$	e_3	0	$-$	$-$
$TB''_{-2,4}(x)$	ℓ_4	e_5	0	$-$	$-$

TABLE 5. The values of $TB_{N-2,4}(x)$, $TB'_{N-2,4}(x)$ and $TB''_{N-2,4}(x)$ at the nodal points.

	x_{N-4}	x_{N-3}	x_{N-2}	x_{N-1}	x_N
$TB_{N-2,4}(x)$	$-$	$-$	0	e_1	0
$TB'_{N-2,4}(x)$	$-$	$-$	0	$-e_3$	$\ell_1 = -\ell_2$
$TB''_{N-2,4}(x)$	$-$	$-$	0	e_5	ℓ_4

Where

$$\ell_1 = -\ell_2 = \frac{-\omega + \omega\cos(\omega h)}{\omega h - \sin(\omega h)}, \quad \ell_4 = \frac{\omega^2 \sin(\omega h)}{\omega h \cos(\omega h) - \sin(\omega h)} - \frac{\omega^2 \sin(\omega h)}{\omega h - \sin(\omega h)},$$

$$e_1 = \frac{-\omega h + \sin(\omega h)}{2\omega h \cos(\omega h) - 2\sin(\omega h)}, \quad e_3 = \frac{\omega \sin^2\left(\frac{\omega h}{2}\right)}{\omega h \cos(\omega h) - \sin(\omega h)}, \quad \text{and}$$

$$e_5 = \frac{\omega^2}{2 - 2\omega h \cot(\omega h)}.$$

TABLE 6. The values of $TB_{-1,4}(x)$, $TB'_{-1,4}(x)$ and $TB''_{-1,4}(x)$ at the nodal points.

	x_0	x_1	x_2	x_3	x_4
$TB_{-1,4}(x)$	0	e_2	η	0	$-$
$TB'_{-1,4}(x)$	0	e_4	$-\rho$	0	$-$
$TB''_{-1,4}(x)$	ℓ_5	e_6	σ	0	$-$

TABLE 7. The values of $TB_{N-3,4}(x)$, $TB'_{N-3,4}(x)$ and $TB''_{N-3,4}(x)$ at the nodal points.

	x_{N-4}	x_{N-3}	x_{N-2}	x_{N-1}	x_N
$TB_{N-3,4}(x)$	$-$	0	η	e_2	0
$TB'_{N-3,4}(x)$	$-$	0	ρ	$-e_4$	0
$TB''_{N-1,4}(x)$	$-$	0	σ	e_6	ℓ_5

Where

$$e_2 = \frac{1}{4}\left[6 + \frac{2\cot\left(\frac{\omega h}{2}\right)}{\omega h} - \frac{1}{\sin^2\left(\frac{\omega h}{2}\right)} + \frac{2\omega h\left(-1 + \cos(\omega h)\right)}{-\omega h \cos(\omega h) + \sin(\omega h)}\right],$$

$$e_4 = \frac{-\omega h + \sin(\omega h)}{2\omega h^2 \cos(\omega h) - 2h \sin(\omega h)},$$

$$e_6 = \frac{1}{2}\left[\frac{\omega^2 \sin(\omega h)}{-\omega h + \omega h \cos(\omega h)} + \frac{\omega^2 \sin(\omega h)}{\omega h \cos(\omega h) - \sin(\omega h)}\right] \quad \text{and}$$

$$\ell_5 = \frac{\omega^2}{1 - \omega h \cot(\omega h)}.$$

3.3. **Cubic UAT Tension B-spline Representation.** Using cubic UAT tension B-splines, we approximate the solution of the SPBVPs (1.1) as follows:

Let $Z(x)$ be a cubic UAT tension B-spline defined over the knot sequence Δ. The function $Z(x)$ can be expressed as a linear combination of cubic UAT tension B-spline basis functions:

$$Z(x) = \sum_{j=-3}^{N-1} c_j TB_j(x), \tag{3.4}$$

where the real coefficients c_j are unknown, and $TB_j(x) = TB_{j,4}(x)$ are the cubic UAT tension B-spline functions.

The values and derivatives of the UAT tension B-splines, provided in Tables 1 to 7, are used to solve the SPBVPs (1.1). At the nodal points, the following conditions hold:

At x_0:

$$\begin{cases} Z(x_0) = c_{-3} = A_0, \\ Z'(x_0) = \ell_1(c_{-3} - c_{-2}), \\ Z''(x_0) = \ell_3 c_{-3} + \ell_4 c_{-2} + \ell_5 c_{-1}. \end{cases} \tag{3.5}$$

At x_1:

$$\begin{cases} Z(x_1) = e_1 c_{-2} + e_2 c_{-1} + \eta c_0, \\ Z'(x_1) = e_3 c_{-2} + e_4 c_{-1} + \rho c_0, \\ Z''(x_1) = e_5 c_{-2} + e_6 c_{-1} + \sigma c_0. \end{cases} \tag{3.6}$$

At x_i for $i = 2, 3, \ldots, N-2$:

$$\begin{cases} Z(x_i) = \eta c_{i-3} + \kappa c_{i-2} + \eta c_{i-1}, \\ Z'(x_i) = -\rho(c_{i-3} - c_{i-1}), \\ Z''(x_i) = \sigma(c_{i-3} - 2c_{i-2} + c_{i-1}). \end{cases} \tag{3.7}$$

At x_{N-1}:

$$\begin{cases} Z(x_{N-1}) = \eta c_{N-4} + e_2 c_{N-3} + e_1 c_{N-2}, \\ Z'(x_{N-1}) = -\rho c_{N-4} - e_4 c_{N-3} - e_3 c_{N-2}, \\ Z''(x_{N-1}) = \sigma c_{N-4} + e_6 c_{N-3} + e_5 c_{N-2}. \end{cases} \tag{3.8}$$

At x_N:

$$\begin{cases} Z(x_N) = c_{N-1} = A_1, \\ Z'(x_N) = \ell_1(c_{N-2} - c_{N-1}), \\ Z''(x_N) = \ell_5 c_{N-3} + \ell_4 c_{N-2} + \ell_3 c_{N-1}. \end{cases} \tag{3.9}$$

The difference equation associated with the SPBVPs (1.1) at the nodal points is given by:

$$L(Z) \equiv -\varepsilon Z''(x_i) + p(x_i)Z'(x_i) + q(x_i)Z(x_i) = g(x_i), \tag{3.10}$$

where $p(x)$, $q(x)$, and $g(x)$ at the knots x_i are represented by $p_i = p(x_i)$, $q_i = q(x_i)$, and $g_i = g(x_i)$.

Substituting the conditions from (3.5) to (3.9) into the operator L (3.10), we get the system of equations that follows:
At x_0:

$$\begin{cases} -\varepsilon(\ell_3 c_{-3} + \ell_4 c_{-2} + \ell_5 c_{-1}) + p_0(\ell_1 c_{-3} + \ell_2 c_{-2}) + q_0 c_{-3} = g_0, \\ (-\varepsilon\ell_3 + p_0\ell_1 + q_0)c_{-3} + (-\varepsilon\ell_4 + p_0\ell_2)c_{-2} - (\varepsilon\ell_5)c_{-1} = g_0. \end{cases} \tag{3.11}$$

At x_1:

$$\begin{cases} -\varepsilon(e_5 c_{-2} + e_6 c_{-1} + \sigma c_0) + p_1(e_3 c_{-2} + e_4 c_{-1} + \rho c_0) + q_1(e_1 c_{-2} + e_2 c_{-1} + \eta c_0) = g_1, \\ (-\varepsilon e_5 + p_1 e_3 + q_1 e_1)c_{-2} + (-\varepsilon e_6 + p_1 e_4 + q_1 e_2)c_{-1} + (-\varepsilon\sigma + p_1\rho + q_1\eta)c_0 = g_1. \end{cases} \tag{3.12}$$

At x_i for $i = 2, \ldots, N-2$:

$$\begin{cases} -\varepsilon\sigma(c_{i-3} - 2c_{i-2} + c_{i-1}) + p_i\rho(-c_{i-3} + c_{i-1}) + q_i(\eta c_{i-3} + \kappa c_{i-2} + \eta c_{i-1}) = g_i, \\ (-\varepsilon\sigma - p_i\rho + q_i\eta)c_{i-3} + (2\varepsilon\sigma + q_i\kappa)c_{i-2} + (-\varepsilon\sigma + p_i\rho + q_i\eta)c_{i-1} = g_i. \end{cases} \tag{3.13}$$

At x_{N-1}:

$$\begin{cases} -\varepsilon(\sigma c_{N-4} + e_6 c_{N-3} + e_5 c_{N-2}) + p_{N-1}(-\rho c_{N-4} - e_4 c_{N-3} - e_3 c_{N-2}) \\ +q_{N-1}(\eta c_{N-4} + e_2 c_{N-3} + e_1 c_{N-2}) = g_{N-1}, \\ (-\varepsilon\sigma - p_{N-1}\rho + q_{N-1}\eta)c_{N-4} + (-\varepsilon e_6 - p_{N-1}e_4 + q_{N-1}e_2)c_{N-3} \\ +(-\varepsilon e_5 - p_{N-1}e_3 + q_{N-1}e_1)c_{N-2} = g_{N-1}. \end{cases} \tag{3.14}$$

At x_N:

$$\begin{cases} -\varepsilon(\ell_5 c_{N-3} + \ell_4 c_{N-2} + \ell_3 c_{N-1}) + p_N(-\ell_2 c_{N-2} - \ell_1 c_{N-1}) + q_N c_{N-1} = g_N, \\ (-\varepsilon\ell_5)c_{N-3} + (-\varepsilon\ell_4 - p_N\ell_2)c_{N-2} + (-\varepsilon\ell_3 - p_N\ell_1 + q_N)c_{N-1} = g_N. \end{cases} \tag{3.15}$$

By removing c_{-3} from (3.11) and c_{N-1} from (3.15), we obtain:
At x_0:

$$\begin{cases} c_{-3} = A_0, \\ (-\varepsilon\ell_4 + p_0\ell_2)c_{-2} - (\varepsilon\ell_5)c_{-1} = g_0 - (-\varepsilon\ell_3 + p_0\ell_1 + q_0)A_0. \end{cases} \tag{3.16}$$

At x_N:

$$\begin{cases} c_{N-1} = A_1, \\ (-\varepsilon\ell_5)c_{N-3} + (-\varepsilon\ell_4 - p_N\ell_2)c_{N-2} = g_N - (-\varepsilon\ell_3 - p_N\ell_1 + q_N)A_1. \end{cases} \tag{3.17}$$

Equations (3.16) and (3.17) can be coupled with the $(N-1)$ equations from (3.12) to (3.14), yielding a system of $(N+1)$ linear equations in $(N+1)$ unknowns. This system can be expressed in matrix-vector form as:

$$H\,C = G,$$

where the matrix H is $(N+1)\times(N+1)$, and C and G are $(N+1)\times 1$ column matrices defined as follows:

$$\begin{pmatrix} m_1 & m_2 & 0 & 0 & \dots & 0 & 0 & 0 & 0 \\ m_3 & m_4 & m_5 & 0 & \dots & 0 & 0 & 0 & 0 \\ 0 & \alpha_2 & \beta_2 & \gamma_2 & \dots & 0 & 0 & 0 & 0 \\ \vdots & \vdots & \vdots & \vdots & \ddots & \vdots & \vdots & \vdots & \vdots \\ 0 & 0 & 0 & 0 & \dots & \alpha_{N-2} & \beta_{N-2} & \gamma_{N-2} & 0 \\ 0 & 0 & 0 & 0 & \dots & 0 & m_{50} & m_{40} & m_{30} \\ 0 & 0 & 0 & 0 & \dots & 0 & 0 & m_{20} & m_{10} \end{pmatrix} \begin{pmatrix} c_{-2} \\ c_{-1} \\ c_0 \\ \vdots \\ c_{N-4} \\ c_{N-3} \\ c_{N-2} \end{pmatrix} = \begin{pmatrix} g_0 - m_0 A_0 \\ g_1 \\ g_2 \\ \vdots \\ g_{N-2} \\ g_{N-1} \\ g_N - m_{00} A_1 \end{pmatrix}, \tag{3.18}$$

where the coefficients α_i, β_i, γ_i, m_0, m_1, m_2, m_3, m_4, m_5, m_{00}, m_{10}, m_{20}, m_{30}, m_{40}, and m_{50} are defined as:

$$\begin{aligned} \alpha_i &= -\varepsilon\sigma - p_i\rho + q_i\eta, & m_5 &= -\varepsilon\sigma + p_1\rho + q_1\eta, \\ \beta_i &= 2\varepsilon\sigma + q_i\kappa, & m_{00} &= -\varepsilon\ell_3 - p_N\ell_1 + q_N, \\ \gamma_i &= -\varepsilon\sigma + p_i\rho + q_i\eta, & m_{10} &= -\varepsilon\ell_4 - p_N\ell_2, \\ m_0 &= -\varepsilon\ell_3 + p_0\ell_1 + q_0, & m_{20} &= -\varepsilon\ell_5, \\ m_1 &= -\varepsilon\ell_4 + p_0\ell_2, & m_{30} &= -\varepsilon e_5 - p_{N-1}e_3 + q_{N-1}e_1, \\ m_2 &= \varepsilon\ell_5, & m_{40} &= -\varepsilon e_6 - p_{N-1}e_4 + q_{N-1}e_2, \\ m_3 &= -\varepsilon e_5 + p_1 e_3 + q_1 e_1, & m_{50} &= -\varepsilon\sigma - p_{N-1}\rho + q_{N-1}\eta. \\ m_4 &= -\varepsilon e_6 + p_1 e_4 + q_1 e_2, \end{aligned}$$

The cubic UAT tension B-spline approximation for the SPBVPs (1.1) is obtained using (3.4), where the coefficients c_i satisfy the system defined in (3.18). This system can be solved to determine the coefficients c_i, which in turn provide the approximate solution $Z(x)$.

4. Analysis of Convergence

This section discusses the convergence analysis of the UAT tension B-spline collocation method. Let's start by looking at the lemma that illustrates the property of the set of cubic tension UAT B-splines.

Lemma 4.1. *The following inequality is satisfied by the UAT tension B-spline* $\{TB_i(x)\}_{i=-3}^{N-1}$*:*

$$\sum_{i=-3}^{N-1} |TB_i(x)| \le \frac{5}{3}, \quad x \in [0,1].$$

Proof. According to Table 1, for a particular node x_i, we have

$$\begin{aligned} \sum_{i=-3}^{N-1} |TB_i(x)| &= |TB_{i-1}(x)| + |TB_i(x)| + |TB_{i+1}(x)| \\ &= |\eta| + |\kappa| + |\eta|, \end{aligned}$$

where

$$\eta = \frac{\omega h - \sin(\omega h)}{2\omega h(1-\cos(\omega h))}, \quad \kappa = 1 - \frac{\omega h - \sin(\omega h)}{\omega h(1-\cos(\omega h))}.$$

Using the Taylor series expansions:

$$2\omega h(1-\cos(\omega h)) = (\omega h)^3 - \frac{(\omega h)^5}{12} + \mathcal{O}((\omega h)^7),$$

$$\omega h - \sin(\omega h) = \frac{(\omega h)^3}{6} - \frac{(\omega h)^5}{120} + \mathcal{O}((\omega h)^7),$$

we obtain:

$$\left|\frac{\omega h - \sin(\omega h)}{2\omega h(1-\cos(\omega h))}\right| \leq \frac{1}{6}, \qquad \left|1 - \frac{\omega h - \sin(\omega h)}{\omega h(1-\cos(\omega h))}\right| \leq \frac{2}{3}.$$

Considering the aforementioned, we deduce that:

$$\sum_{i=-3}^{N-1} |TB_i(x)| \leq \frac{5}{3}.$$

Now, for any point $x \in [x_{i-1}, x_i]$, we have:

$$\begin{aligned}
\sum_{i=-3}^{N-1} \mid TB_i\,(x) \mid &= \mid TB_{i-2}\,(x) \mid + \mid TB_{i-1}\,(x) \mid + \mid TB_i\,(x) \mid + \mid TB_{i+1}\,(x) \mid \\
&= 2 \mid \frac{\omega h - sin\,(\omega h)}{2\,\omega h\ (1 - cos\,(\omega h))} \mid +2 \mid 1 - \left[\frac{\omega h - sin\,(\omega h)}{\omega h\ (1 - cos\,(\omega h))}\right] \mid \\
&\leq \left(2 \times \frac{1}{6}\right) + \left(2 \times \frac{2}{3}\right) \\
&\leq \frac{5}{3}
\end{aligned}$$

The proof is so finished. □

Theorem 4.2. *Assume that $Z(x)$ is the collocation approximation to the solution $z(x)$ of the SPBVPs 1.1. Next, assuming N is large enough, we get the ε-uniform error estimate as follows:*

$$\sup_{0<\varepsilon\leq 1} \|Z - z\|_{\bar{\Omega}} \leq CN^{-2}(\ln(N))^2,$$

where C is a constant that doesn't depend on ε.

Proof. The discrete problem's solution Z can be decomposed as

$$Z = R + S.$$

where R is the regular component and S is the singular component, as described in [8].

$$LR = f, \quad R(0) = r(0), \quad R(1) = r(1).$$

and

$$LS = 0, \quad S(0) = s(0), \quad S(1) = s(1).$$

Consequently, the error can be expressed using the form

$$Z - z = (R - r) + (S - s).$$

The ε-uniform error estimate is obtained here by using the spline interpolation error estimates of de Boor [3] and Hall [7]. We arrive at the following ε-uniform error estimate by employing de Boor-Hall error estimates, matrix analysis, and simplification:

$$\sup_{0<\varepsilon\leq 1} \|Z - z\| \leq C(h^*)^2 \max_{\Omega} |z''|, \tag{4.1}$$

where $h^* = \max\{h_\ell, h_r\}$.
On each subinterval $\Omega_i = [x_{i-1}, x_i]$, where $i = 1, 2, \ldots, N$, the ε-uniform convergence estimate is obtained.
The four cubic UAT B-splines that cover each subinterval Ω_i are as follows:

$$Z = c_{i-2}TB_{i-2}(x) + c_{i-1}TB_{i-1}(x) + c_iTB_i(x) + c_{i+1}TB_{i+1}(x).$$

The following is evident on Ω_i:

$$|Z(x)| \leq \max_{\Omega_i} |z(x)| \,. \tag{4.2}$$

From the ε-uniform error estimate (4.1), we have:

$$|Z(x) - z(x)| \leq C h_i^2 \max_{\Omega_i} |z''| \,. \tag{4.3}$$

The following estimates are valid for the solution z of (1.1) and its derivatives according to Lemma (2.3)

$$\left| z^{(k)}(x) \right| \leq C \varepsilon^{-k}, \quad for \;\; 0 \leq k \leq 3.$$

Thus, using Eq.(4.3), we obtain

$$|Z(x) - z(x)| \leq C \frac{h_i^2}{\varepsilon^2}. \tag{4.4}$$

Additionally, applying Eqs. (4.2) and (4.3) to Ω_i, we obtain

$$\begin{aligned} |Z(x) - z(x)| &= |R(x) + S(x) - r(x) - s(x)| \\ &\leq |R(x) - r(x)| + |S(x) - s(x)| \\ &\leq C\, h_i^2 \, \underset{\Omega_i}{max} \left| r''(x) \right| + 2 \, \underset{\Omega_i}{max} \, |s(x)| \\ &\leq C \left(h_i^2 + exp\left(\frac{-p^* (1 - x_i)}{\varepsilon} \right) \right). \end{aligned} \tag{4.5}$$

Because, according to Theorem (2.4), we have

$$\left| r''(x) \right| \leq C \left[1 + exp\left(\frac{-p^* (1 - x)}{\varepsilon} \right) \right], \quad \forall x \in \bar{\Omega} = [0, 1] \,.$$

and

$$|s(x)| \leq C \, exp\left(\frac{-p^* (1 - x)}{\varepsilon} \right), \quad \forall x \in \bar{\Omega} = [0, 1] \,.$$

In order to estimate the ε-uniform error, we now examine two different cases separately:

$$\Upsilon_0 \, \varepsilon \, ln(N) \geq \frac{1}{2} \quad or \quad \Upsilon_0 \, \varepsilon \, ln(N) \leq \frac{1}{2}$$

.

Case 1. $\Upsilon_0 \, \varepsilon \, ln(N) \geq \frac{1}{2}$, so we have transition parameter $\Upsilon = \frac{1}{2}$.
In this case $h = \frac{1}{N}$ and $\frac{1}{\varepsilon} \leq C \, ln(N)$.
Consequently, we obtain ε-uniform estimates using the inequality (4.4).

$$|Z(x) - z(x)| \leq C \, N^{-2} \, (ln(N))^2 \,, \quad i = 0, 1, \ldots, N.$$

Case 2. $\Upsilon_0 \, \varepsilon \, ln(N) \leq \frac{1}{2}$, thus, we have $\Upsilon = \Upsilon_0 \, \varepsilon \, ln(N)$ as the transition parameter. In the present case, $h_i = \frac{2\Upsilon}{N}$ for i satisfies $\frac{N.}{2} + 1 \leq i \leq N$ in the boundary layer region, and the mesh is piecewise uniform. Therefore

$$\frac{h_i}{\varepsilon} = \frac{2\Upsilon}{N\varepsilon} = C \, N^{-1} \, ln(N) \,, \quad \frac{N.}{2} + 1 \leq i \leq N.$$

Thus, the inequality (4.4) yields

$$|Z(x) - z(x)| \leq C \, N^{-2} \, (ln(N))^2 \,, \quad \frac{N.}{2} + 1 \leq i \leq N.$$

However, if i satisfies $1 \le i \le \frac{N}{2}$ in a region without a boundary layer, then $\Upsilon \le 1 - x_i$ and hence

$$exp\left(\frac{-p^*\left(1-x_i\right)}{\varepsilon}\right) \le exp\left(\frac{-p^*\Upsilon}{\varepsilon}\right) = exp\left(-p^*\,\Upsilon_0\,ln\left(N\right)\right) = N^{-p^*\,\Upsilon_0} = N^{-2}.$$

when $\Upsilon_0 = \frac{2}{p^*}$ is used in the transition parameter Υ definition. The inequality (4.5) gives

$$\begin{aligned} \left|Z\left(x\right) - z\left(x\right)\right| &\le C\left(h_i^2 + exp\left(\frac{-\alpha\left(1-x_i\right)}{\varepsilon}\right)\right) \\ &\le C\,N^{-2}\,\left(ln\left(N\right)\right)^2. \end{aligned}$$

The method is therefore uniformly convergent of order two in the discrete maximum norm. Thus, the proof is finished. □

5. Numerical examples, results and discussions

In this section, we present three numerical examples to demonstrate the efficiency and accuracy of our method. The results and discussions of these numerical examples will be compared with those provided in [8] and [14].
The maximum pointwise errors E_ε^N, shown in the tables for various values of ε and N, are determined by the following formula:

$$E_\varepsilon^N = \max_{x_i \in \bar{\Omega}_N} \left|z\left(x_i\right) - Z^N\left(x_i\right)\right|,$$

where $z\left(x_i\right)$ and $Z^N\left(x_i\right)$ represent the exact and approximate solutions of the given problem at x_i, respectively.
Additionally, the numerical order of convergence is calculated using the formula:

$$r_\varepsilon^N = \frac{ln\left(E_\varepsilon^N\right) - ln\left(E_\varepsilon^{2N}\right)}{ln\,2}.$$

Example 5.1. Consider the following non-homogeneous SPBVPs [8]:

$$\begin{cases} -\varepsilon\,z''\left(x\right) + z'\left(x\right) + z\left(x\right) = \cos\left(x\right), \quad x \in \Omega = [0,1]. \\ z\left(0\right) = 0 \quad, z\left(1\right) = 0. \end{cases} \tag{5.1}$$

which has the analytical solution given by

$$z\left(x\right) = a_1\,\cos\left(\pi x\right) + a_2\,\sin\left(\pi x\right) + A_1\,\exp\left(\xi_1 x\right) + A_2\,\exp\left(-\xi_2\left(1-x\right)\right).$$

where $\xi_1 < 0$ and $\xi_2 > 0$ constitute the characteristic equation's real solutions:

$$-\varepsilon\,\xi^2 + \xi + 1 = 0.$$

and

$$a_1 = \frac{\varepsilon\,\pi^2 + 1}{\pi^2 + \left(\varepsilon\,\pi^2 + 1\right)^2}, \quad a_2 = \frac{\pi}{\pi^2 + \left(\varepsilon\,\pi^2 + 1\right)^2}$$

$$A_1 = -a_1\,\frac{1 + \exp\left(-\xi_1\right)}{1 - \exp\left(\xi_0 - \xi_1\right)}, \quad A_2 = a_1\,\frac{1 + \exp\left(\xi_0\right)}{1 - \exp\left(\xi_0 - \xi_1\right)}.$$

Example 5.2. Now consider the following homogeneous SPBVPs [8]:

$$\begin{cases} -\varepsilon\, z''(x) + z'(x) + (1+\varepsilon)\, z(x) = 0, & x \in \Omega = [0,1]. \\ z(0) = 1 + \exp\left[-\frac{(1+\varepsilon)}{\varepsilon}\right],\ z(1) = 1 + \exp\left[\frac{1}{\exp(1)}\right]. \end{cases} \tag{5.2}$$

The exact solution of this problem is

$$z(x) = \exp\left[\frac{(1+\varepsilon)(x-1)}{\varepsilon}\right] + \exp(-x).$$

Example 5.3. Let us consider the following SPBVPs see Lin *et al.*[14]:

$$\begin{cases} -\varepsilon\, z''(x) + z'(x) + z(x) = 1, \quad x \in \Omega = [0,1] \\ \quad z(0) = 0 \quad, z(1) = 0 \end{cases} \tag{5.3}$$

The exact solution is given by

$$z(x) = \exp(\theta_1 x)\left(\frac{\exp(\theta_2) - 1}{\exp(\theta_1) - \exp(\theta_2)}\right) + \exp(\theta_2 x)\left(\frac{1 - \exp(\theta_1)}{\exp(\theta_1) - \exp(\theta_2)}\right) + 1.$$

where

$$\theta_1 = \frac{1 + \sqrt{1 + 4\varepsilon}}{2\varepsilon} \quad \text{and} \quad \theta_2 = \frac{1 - \sqrt{1 + 4\varepsilon}}{2\varepsilon}.$$

Tables 8–10 present the maximum absolute error E_ε^N and the rate of convergence r_ε^N for the considered examples 1 to 3 for different values of ε and N. These tables allow us to observe the following:

- The values of the errors E_ε^N decrease as N increases for a fixed value of ε. In relation to the mesh parameter, this indicates that the convergence is uniform.
- Errors E_ε^N decrease with increasing N, regardless of perturbation ε values. This illustrates how the suggested approach converges ε-uniformly.
- The theoretical estimations are supported by numerical results, and the current approach is second order accurate.

TABLE 8. The errors E_ε^N and r_ε^N of Example 1 for different N and ε values.($\omega = 3.1$)

ε	The mesh intervals' number N						
	16	32	64	128	256	512	
10^0	$7.136e-05$	$1.778e-05$	$4.444e-06$	$1.111e-06$	$2.777e-07$	$6.942e-08$	E_ε^N
	2.0049	2.0001	2.0003	2.0000	1.9999	–	r_ε^N
10^{-1}	$2.845e-03$	$7.237e-04$	$1.792e-04$	$4.469e-05$	$1.117e-05$	$2.792e-06$	E_ε^N
	1.9750	2.0137	2.0034	2.0007	1.9999	–	r_ε^N

TABLE 9. The errors E_ε^N and r_ε^N of Example 2 for different N and ε values. ($\omega = 0.7$)

ε	The mesh intervals' number N						
	16	32	64	128	256	512	
10^0	$2.158e-04$	$5.277e-05$	$1.306e-05$	$3.249e-06$	$8.106e-07$	$2.024e-07$	E_ε^N
	2.032	2.0145	2.0067	2.0029	2.0032	–	r_ε^N
10^{-4}	$2.918e-02$	$1.469e-02$	$6.818e-03$	$2.773e-03$	$1.230e-03$	$5.875e-04$	E_ε^N
	0.9904	1.1073	1.2977	1.1727	1.0662	–	r_ε^N

TABLE 10. The errors E_ε^N and r_ε^N of Example 3 for different N and ε values. ($\omega = 0.1$)

ε	The mesh intervals' number N						
	16	32	64	128	256	512	
10^0	$6.494e-05$	$1.624e-05$	$4.061e-06$	$1.015e-06$	$2.538e-07$	$6.345e-08$	E_ε^N
	1.9998	1.9995	2.0001	1.9999	1.9999	–	r_ε^N
0.0015	$2.529e-02$	$1.011e-02$	$4.190e-03$	$1.814e-03$	$7.108e-04$	$2.475e-04$	E_ε^N
	1.3227	1.2709	1.2081	1.3513	1.5222	–	r_ε^N

In Tables 11–14, the maximum absolute errors of the our method are compared with those of Kadalbajoo *et al.* [8] and Lin *et al.* [14] for Examples 1–3.
These tables show that, in comparison to the methods described in [8] and [14], the current approach yields higher accuracy.

TABLE 11. Comparison of the errors E_ε^N of Example 1 for various N values and $\varepsilon = 10^0$.

N	$\varepsilon = 10^0$		
	Method in [8]	Our method ($\omega = 3.1$)	Our method ($\omega = 1$)
16	$2.3803e-04$	$7.1358e-05$	$1.1693e-04$
32	$5.9435e-05$	$1.7778e-05$	$2.9464e-05$
64	$1.4854e-05$	$4.4442e-06$	$7.3671e-06$
128	$3.7133e-06$	$1.1108e-06$	$1.8418e-06$
256	$9.284e-07$	$2.7769e-07$	$4.6047e-07$
512	$2.321e-07$	$6.9423e-08$	$1.1511e-07$
1024	$5.8022e-08$	$1.7355e-08$	$2.8779e-08$

TABLE 12. Comparison of the errors E_ε^N of Example 1 for various N values and $\varepsilon = 10^{-2}$.

N	$\varepsilon = 10^{-2}$		
	Method in [8]	Our method ($\omega = 3.1$)	Our method ($\omega = 1$)
64	$6.6001e-03$	$5.4174e-03$	$5.4137e-03$
128	$2.4825e-03$	$1.1763e-03$	$1.1756e-03$
512	$1.6137e-04$	$1.5757e-04$	$1.5745e-04$

TABLE 13. Comparison of the errors E_ε^N of Example 2 for various N values and $\varepsilon = 10^{-4}$.

N	$\varepsilon = 10^{-4}$		
	Method in [8]	Our method ($\omega = 0.7$)	Our method ($\omega = 1$)
16	$3.2912e-02$	$2.9184e-02$	$2.9213e-02$
128	$2.9970e-03$	$2.7733e-03$	$2.7739e-03$
256	$1.4339e-03$	$1.2302e-03$	$1.2304e-03$

TABLE 14. Comparison of the errors E_ε^N of Example 3 with an equidistant mesh of $N = 128$ ($\omega = 1$).

x	$\varepsilon = 0.5$		$\varepsilon = 0.01$		$\varepsilon = 0.0015$	
	Lin *et al.*[14]	Our method	Lin *et al.*[14]	Our method	Lin *et al.*[14]	Our method
1/16	$4.4e-03$	$5.9231e-07$	$7.3e-03$	$5.4341e-04$	$7.4e-03$	$1.6285e-03$
2/16	$4e-03$	$1.1969e-06$	$6.9e-03$	$4.8563e-04$	$6.9e-03$	$1.4399e-03$
4/16	$3.1e-03$	$2.4293e-06$	$6.1e-03$	$3.8784e-04$	$6.1e-03$	$1.1257e-03$
6/16	$2.2e-03$	$3.6422e-06$	$5.4e-03$	$3.0975e-04$	$5.4e-03$	$8.7887e-04$
12/16	$2.5e-03$	$5.3939e-06$	$3.7e-03$	$1.0837e-03$	$3.7e-03$	$1.6758e-03$
14/16	$5.1e-03$	$3.9436e-06$	$3.3e-03$	$7.6125e-04$	$3.3e-03$	$1.7260e-03$

For both uniform and Shishkin meshes, the errors E_ε^N for various N and ε values is shown in tables 15–17 for the considered examples 1 to 3. Using these tables, we can see the following:

- The maximum absolute error is smaller. This indicates that the numerical solution under Shishkin mesh efficiently and accurately approximates the exact solution.
- When the singularly perturbed effect is high, the numerical solution does not accurately approximate the exact solution under a uniform mesh.

TABLE 15. The errors E_ε^N for uniform and Shishkin meshes in Example 1 ($\omega = 3.1$).

	$N = 64$		$N = 128$		$N = 256$	
ε	Uniform	Shishkin	Uniform	Shishkin	Uniform	Shishkin
10^{-3}	0.0976	0.0152	0.0750	0.0065	0.0435	0.0026
10^{-4}	0.1356	0.0162	0.1194	0.0077	0.1135	0.0038
10^{-5}	0.1977	0.0160	0.1648	0.0075	0.1293	0.0037

TABLE 16. The errors E_ε^N for uniform and Shishkin meshes in Example 2 ($\omega = 0.7$).

	$N = 64$		$N = 128$		$N = 256$	
ε	Uniform	Shishkin	Uniform	Shishkin	Uniform	Shishkin
10^{-3}	0.7692	0.0052	0.5914	0.0021	0.3427	0.0008
10^{-4}	1.0768	0.0068	0.9483	0.0028	0.9014	0.0012
10^{-5}	1.5711	0.0077	1.3095	0.0037	1.0275	0.0016

TABLE 17. The errors E_ε^N for uniform and Shishkin meshes in Example 3 ($\omega = 0.1$).

	$N = 32$		$N = 64$		$N = 128$	
ε	Uniform	Shishkin	Uniform	Shishkin	Uniform	Shishkin
0.0015	0.5163	0.0101	0.4261	0.0042	0.2841	0.0018
0.01	0.1653	0.0073	0.0549	0.0019	0.0125	0.0019
0.5	$8.872e-05$	$8.872e-05$	$2.216e-05$	$2.216e-05$	$5.541e-06$	$5.541e-06$

Figures 2–10 illustrate the numerical solution profiles for Examples 1 to 3 at various values of ε and N. From each figure, we observe the following:

- The boundary layer's existence at $x = 1$.
- As can be seen in Figures 2(a)–10(a), the boundary layer at $x = 1$ causes the numerical solution to not converge to the real solution under a uniform mesh, and there are apparent oscillations as $\varepsilon \to 0$.
- However, our proposed method converges to the true solution under a Shishkin mesh, as shown in Figures 2(b)–10(b).
- Near the transition point, abrupt changes in the mesh size lead to maximum pointwise errors.
- As ε decreases, the boundary layer width τ also decreases, becoming increasingly steeper at $x = 1$. This clearly demonstrates the effect of the parameter ε.
- For sufficiently small values of ε, the proposed scheme with a uniform mesh fails to be uniformly convergent.
- The suggested approach with a Shishkin mesh converges ε-uniformly, independent of the mesh and perturbation parameters.
- The exact solution and the numerical solutions obtained using the Shishkin mesh are in excellent agreement.

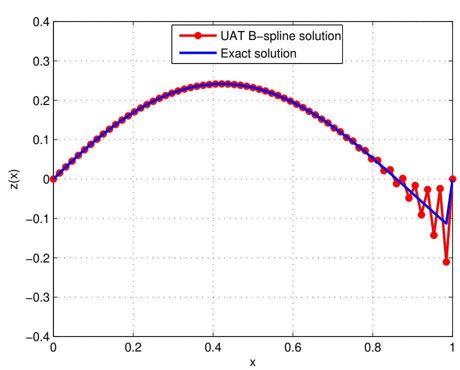

(a) Uniform mesh.

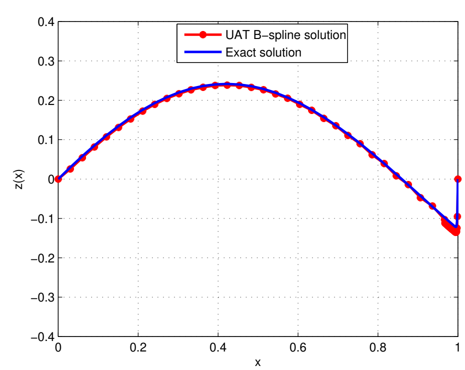

(b) Shishkin mesh.

FIGURE 2. Plotting the solutions for Example 1 with $N = 64$ and $\varepsilon = 10^{-3}$.

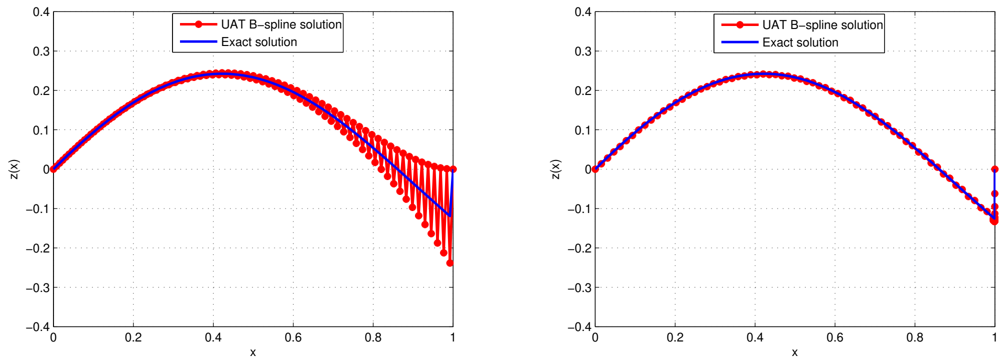

(a) Uniform mesh. (b) Shishkin mesh.

FIGURE 3. Plotting the solutions for Example 1 with $N = 128$ and $\varepsilon = 10^{-4}$.

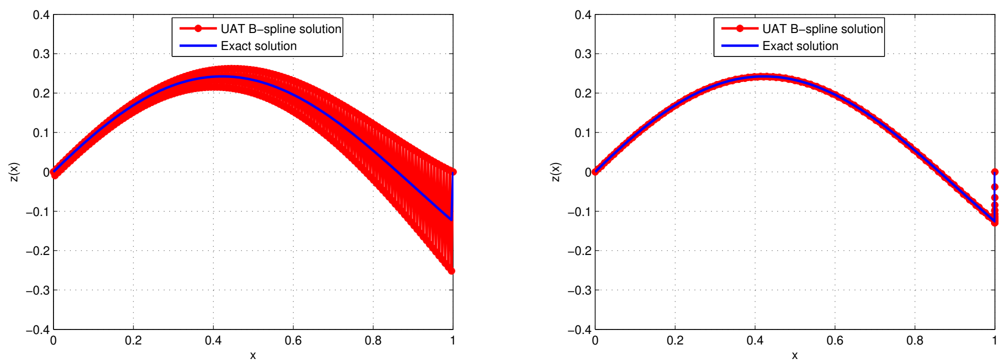

(a) Uniform mesh. (b) Shishkin mesh.

FIGURE 4. Plotting the solutions for Example 1 with $N = 256$ and $\varepsilon = 10^{-5}$.

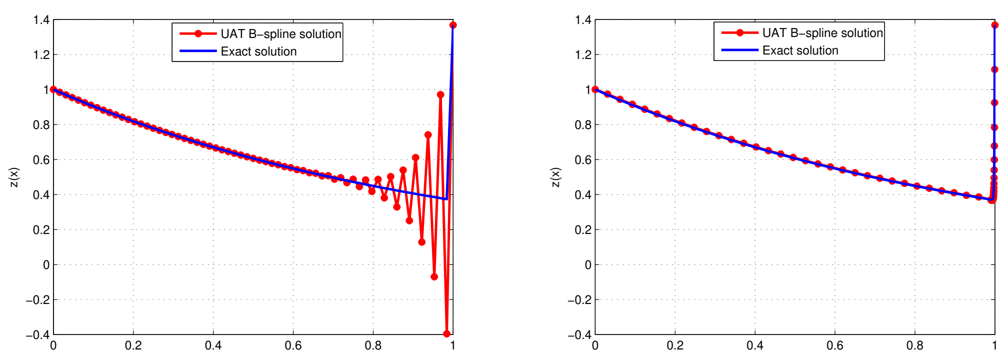

(a) Uniform mesh. (b) Shishkin mesh.

FIGURE 5. Plotting the solutions for Example 2 with $N = 64$ and $\varepsilon = 10^{-3}$.

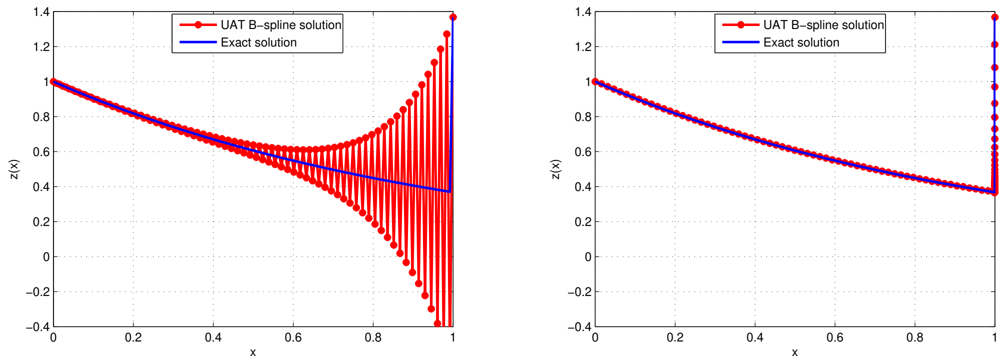

(a) Uniform mesh. (b) Shishkin mesh.

FIGURE 6. Plotting the solutions for Example 2 with $N = 128$ and $\varepsilon = 10^{-4}$.

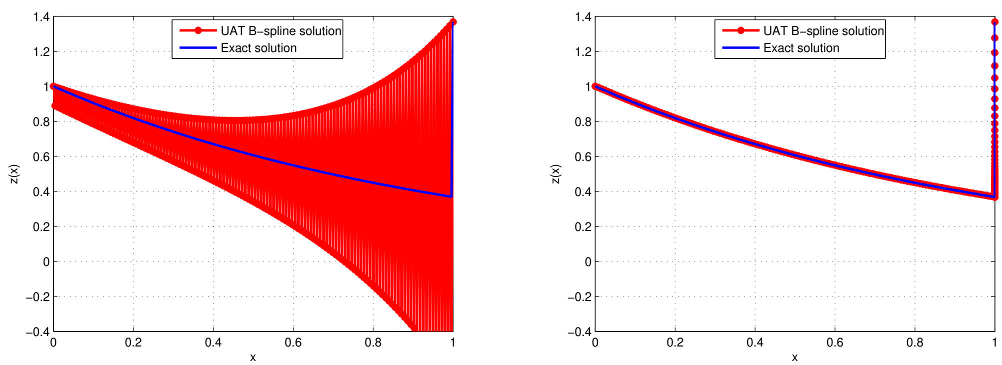

(a) Uniform mesh. (b) Shishkin mesh.

FIGURE 7. Plotting the solutions for Example 2 with $N = 256$ and $\varepsilon = 10^{-5}$.

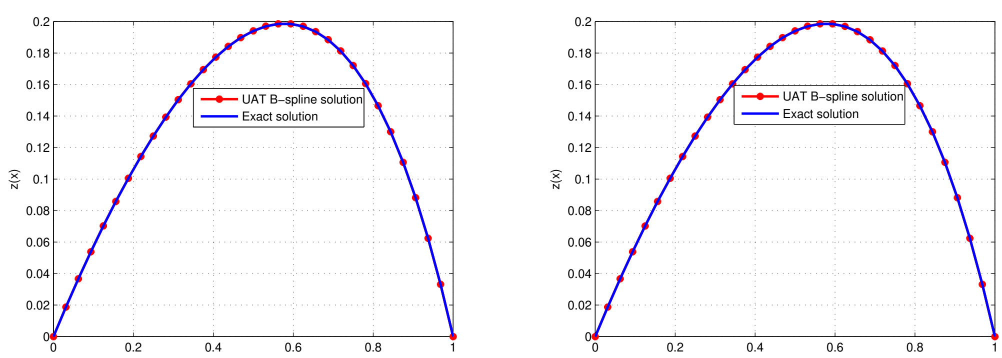

(a) Uniform mesh. (b) Shishkin mesh.

FIGURE 8. Plotting the solutions for Example 3 with $N = 32$ and $\varepsilon = 0.5$.

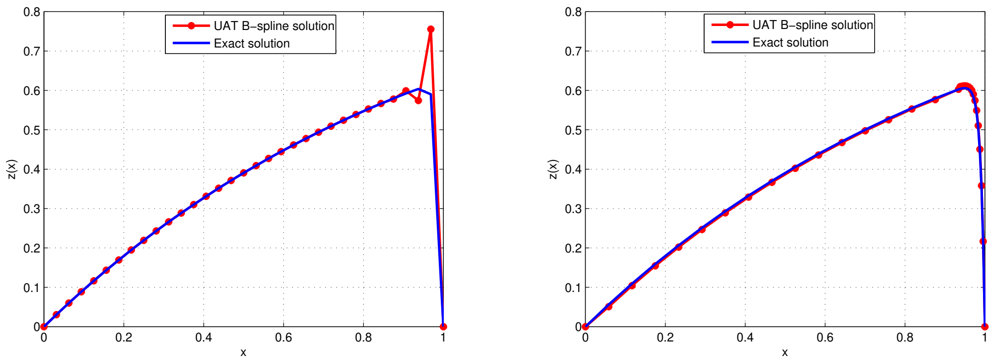

(a) Uniform mesh. (b) Shishkin mesh.

FIGURE 9. Plotting the solutions for Example 3 with $N = 32$ and $\varepsilon = 0.01$.

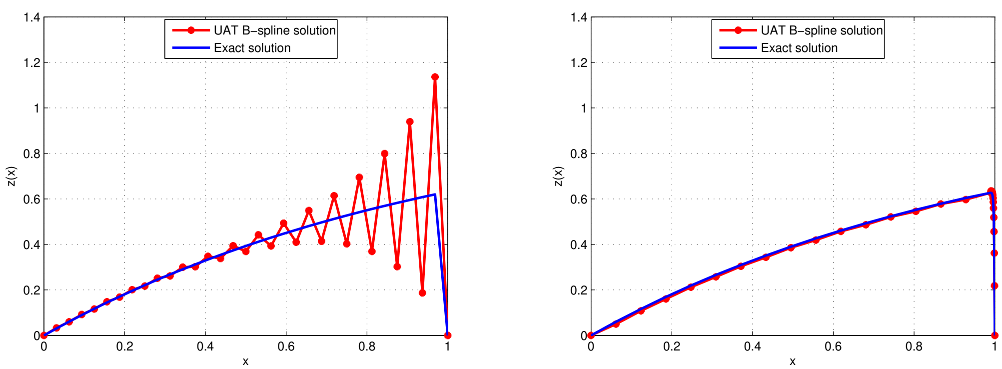

(a) Uniform mesh. (b) Shishkin mesh.

FIGURE 10. Plotting the solutions for Example 3 with $N = 32$ and $\varepsilon = 0.0015$.

6. Conclusion

In this article, the Uniform Algebraic Trigonometric (UAT) tension B-spline method has been effectively employed to numerically solve a class of convection-diffusion problems with singular perturbations. A uniform piecewise mesh is used to discretize the domain. As opposed to other methods, the proposed approach is straightforward to implement and is more economical due to its tridiagonal matrix structure. Three model examples are presented to illustrate the efficiency and accuracy of the suggested approach. The results demonstrate that the suggested scheme offers more accurate solutions compared to some previous findings in the literature. Future work could extend this method to handle problems with two parameters and to higher-dimensional problems.

References

1. Alinia, N. & Zarebnia, M. (2018). A new tension B-spline method for third-order self-adjoint singularly perturbed boundary value problems. Journal of Computational and Applied Mathematics, 342, 521-533. https://doi.org/10.1016/j.cam.2018.03.021

2. Alinia, N. & Zarebnia, M. (2018). Trigonometric tension B-spline method for the solution of problems in calculus of variations. Computational Mathematics and Mathematical Physics, 58(5), 631-641. https://doi.org/10.1134/S0965542518050020
3. De Boor, C. (1968). On the convergence of odd-degree spline interpolation. Journal of approximation theory, 1(4), 452-463. https://doi.org/10.1016/0021-9045(68)90033-6
4. Doolan, E.P., Miller, J.J., & Schilders, W.H. (1980). Uniform numerical methods for problems with initial and boundary layers. Boole Press.
5. Farrell, P., Hegarty, A., Miller, J.M., O'Riordan, E., & Shishkin, G.I. (2000). Robust computational techniques for boundary layers. Chapman and hall/CRC.
6. Hajji, S., Danouj, B., & Lamnii,A. (2018). Uat b-splines of order 4 for reconstructing the curves and surfaces. Applied Mathematical Sciences, 12(21), 1007-1020. https://doi.org/10.12988/ams.2018.87104
7. Hall, C. A. (1968). On error bounds for spline interpolation. Journal of approximation theory, 1(2), 209-218. https://doi.org/10.1016/0021-9045(68)90025-7
8. Kadalbajoo, M.K., & Gupta, V. (2009). Numerical solution of singularly perturbed convection-diffusion problem using parameter uniform B-spline collocation method. Journal of Mathematical Analysis and Applications, 355(1), 439-452. https://doi.org/10.1016/j.jmaa.2009.01.038
9. Kadalbajoo, M.K., & Patidar, K.C. (2002). A survey of numerical techniques for solving singularly perturbed ordinary differential equations. Applied Mathematics and Computation, 130(2-3), 457-510. https://doi.org/10.1016/S0096-3003(01)00112-6
10. Kumar, V., & Srinivasan, B.(2015). An adaptive mesh strategy for singularly perturbed convection diffusion problems. Applied Mathematical Modelling, 39(7), 2081-2091. https://doi.org/10.1016/j.apm.2014.10.019
11. Lamnii, A., Mraoui, H., Sbibih, D., & Zidna, A. (2009). A multiresolution method for fitting scattered data on the sphere. BIT Numerical Mathematics,49(3), 589-610. https://doi.org/10.1007/s10543-009-0230-3
12. Lamnii, A., Mraoui, H., Sbibih, D., & Zidna, A. (2013). Uniform tension algebraic trigonometric spline wavelets of class C2 and order four. Mathematics and Computers in Simulation, 87, 68-86. https://doi.org/10.1016/j.matcom.2012.11.006
13. Lamnii, A., Nour, M. Y., & Zidna, A. (2021). A reverse non-stationary generalized B-splines subdivision scheme. Mathematics, 9, 2628. https://doi.org/10.3390/math9202628
14. Lin, B., Li, K., & Cheng, Z. (2009). B-spline solution of a singularly perturbed boundary value problem arising in biology. Chaos, Solitons and Fractals, 42(5), 2934-2948. https://doi.org/10.1016/j.chaos.2009.04.036
15. Miller, J.J., O'riordan, E., & Shishkin, G.I. (1996). Fitted numerical methods for singular perturbation problems: error estimates in the maximum norm for linear problems in one and two dimensions. World scientific.
16. Robert Jr, E. (2012). Singular perturbation methods for ordinary differential equations. (Vol. 89). Springer Science & Business Media.
17. Ṙoos, H. G., Stynes, M., & Tobiska, L. (2008). Robust numerical methods for singularly perturbed differential equations: convection-diffusion-reaction and flow problems. Berlin, Heidelberg: Springer Berlin Heidelberg.
18. Wang, G., & Fang, M. E. (2008). Unified and extended form of three types of splines. Journal of computational and applied mathematics, 216(2), 498-508. https://doi.org/10.1016/j.cam.2007.05.031
19. Wang, G., & Li, Y. (2006). Optimal properties of the uniform algebraic trigonometric B-splines. Computer Aided Geometric Design, 23(2), 226-238. https://doi.org/10.1016/j.cagd.2005.09.002

[1] University of Abdelmalek Essaadi, laboratory ISI, ENSATe, Tetouan, Morocco.

Email address: mohamed.chaher@etu.uae.ac.ma

[1*] University of Abdelmalek Essaadi, laboratory ISI, ENSATe, Tetouan, Morocco.
Email address: a.lamnii@uae.ac.ma

[2] University of Lorraine, CNRS, Inria, laboratory LORIA, Nancy, France.
Email address: mohamedyassir.nour@gmail.com